HHS Public Access

Author manuscript

FASEB J. Author manuscript; available in PMC 2022 October 01.

Published in final edited form as:

FASEB J. 2021 October ; 35(10): e21873. doi:10.1096/fj.202100731R.

Neuronal Calcium Sensor 1 (NCS1) Dependent Modulation of Neuronal Morphology and Development

Tom T. Fischer[1,2], **Lien D. Nguyen**[1,3,#], **Barbara E. Ehrlich**[1,3,4,*]

[1]Department of Pharmacology, Yale University, 06511 New Haven CT, USA

[2]Institute of Pharmacology, Heidelberg University, 69120 Heidelberg, Germany

[3]Interdepartmental Neuroscience Program, Yale University, 06511 New Haven CT, USA

[4]Department of Physiology, Yale University, 06511 New Haven CT, USA

Abstract

Calcium (Ca2+) signaling is critical for neuronal functioning and requires the concerted interplay of numerous Ca2+-binding proteins, including neuronal calcium sensor 1 (NCS1). Although an important role of NCS1 in neuronal processes and in neurodevelopmental and neurodegenerative diseases has been established, the underlying mechanisms remain enigmatic. Here, we systematically investigated the functions of NCS1 in the brain. Using Golgi-Cox staining, we observed a reduction in dendritic complexity and spine density in the prefrontal cortex and the dorsal hippocampus of *Ncs1*$^{-/-}$ mice, which may underlie concomitantly observed deficits in memory acquisition. Subsequent RNA sequencing of *Ncs1*$^{-/-}$ and *Ncs1*$^{+/+}$ mouse brain tissues revealed that NCS1 modulates gene expression related to neuronal morphology and development. Investigation of developmental databases further supported a molecular role of NCS1 during brain development by identifying temporal gene expression patterns. Collectively, this study provides insights into NCS1-dependent signaling and lays the foundation for a better understanding of NCS1-associated diseases.

Graphical Abstract:

*Corresponding author: 333 Cedar Street, New Haven, CT 06520-8066, USA, barbara.ehrlich@yale.edu, +1 (203) 737 1158.
#Current address: Department of Neurology, Ann Romney Center for Neurologic Diseases, Brigham and Women's Hospital and Harvard Medical School, Boston MA, USA

Author Contributions

T.T.F., L.D.N., B.E.E. designed research; T.T.F. and L.D.N. performed experiments; T.T.F. analyzed the data; L.D.N. contributed analytic tools; T.T.F. wrote the first draft of the manuscript; T.T.F., L.D.N., B.E.E. edited the manuscript; all authors agreed to the final version of the manuscript.

Conflict of Interest statement

B.E.E is a founder of Osmol Therapeutics, a company that is targeting NCS1 for therapeutic purposes. The remaining authors have declared that no conflict of interest exists.

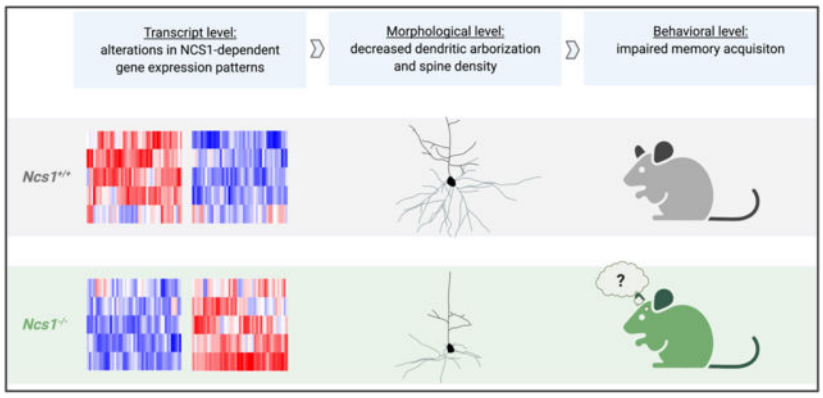

Keywords

calcium signaling; dendritic arborization; neurodevelopment; neurological disease; RNA-Sequencing

Introduction

Tightly regulated calcium (Ca2+) signaling systems are critical for many neuronal processes – from fetal neurogenesis to cognitive functions in adults (1, 2). Consequently, disrupted neuronal Ca2+ signaling has been implicated in the pathophysiology of neurodevelopmental, psychiatric, and neurodegenerative diseases (3–5). For the regulation of neuronal processes, such as neuronal maturation, activity, and plasticity, the concerted interplay of many Ca2+ signaling pathways is crucial (1). Particularly, the EF-hand Ca2+ sensor proteins of the calmodulin (CaM) superfamily are essential for the transduction of Ca2+ signals (6). This study focuses on neuronal calcium sensor 1 (NCS1), one member of the Ca2+ sensor family.

NCS1 is a high affinity, low-capacity Ca2+ binding protein that is ubiquitously expressed, with the highest abundance in neuronal tissues (7). It was first discovered as frequenin (Frq), a protein that enhances frequency-dependent neurotransmitter release, in Drosophila (8). NCS1 primarily transduces Ca2+ signals through interaction with its target proteins, including the D2 dopamine receptor (D2Rs), the voltage-gated Ca2+ channels (Ca_Vs), and the inositol 1,4,5-trisphosphate receptors (InsP3Rs), which exert numerous downstream effects (7, 9–11). As such, NCS1 modulates neurotransmission (8, 12), synaptic plasticity (13–15), neurite outgrowth (16–18), and neuronal survival (18, 19). Knockout of *Ncs1* (*Ncs1*$^{-/-}$) results in a neurological phenotype with impaired memory and learning as observed in *C. elegans* (20) and two mouse strains (15, 21). In contrast, overexpression of NCS1 in the dentate gyrus enhances synaptic plasticity and memory in mice (14). NCS1 has also been demonstrated to play an important role in diseases like autism spectrum disorder (ASD) (22), fragile X syndrome (FXS) (23), Parkinson's disease (24, 25), Alzheimer's disease (26), Wolfram syndrome (27–29), bipolar disorder, and schizophrenia (30, 31). Moreover, NCS1 has been characterized as a promising drug target in several *in vivo* and *in*

vitro models of these diseases (23, 26, 27, 32). However, despite its established significance in neuronal functions and neurological diseases, the precise cellular and molecular functions of NCS1 remain enigmatic.

Here, we combine RNA sequencing (RNA-Seq), Golgi-Cox staining, behavioral experiments, and data-mining strategies to further investigate NCS1-dependent signaling and its implications at the cellular and organismal levels. In *Ncs1*$^{-/-}$ mice, we confirmed deficits in memory acquisition, observed reduced dendritic complexity and spine density, and identified differential gene expression patterns. Moreover, investigations of developmental databases point to a novel molecular function of NCS1 in neurodevelopment.

Materials and Methods

Animal use and treatment.

The *Ncs1* knockout (*Ncs1*$^{-/-}$) mouse strain on the C57Bl6/J background was generated previously and was a kind gift from O. Pongs (Homburg, Germany) (33, 34). Briefly, *Ncs1* was knocked-out in all tissues through gene targeting with a Cre/loxP recombination system that resulted in a loss of four translated exons (exons 4, 5, 6, 7) of *Ncs1* (Fig. 1B–C) and consequently, a complete loss of NCS1 protein (Fig. 1D). This study was carried out in accordance with the recommendations in the U.S. National Institutes of Health Guide for the Care and Use of Laboratory Animals and approved by the Institutional Animal Care and Use Committee at Yale University. All efforts were made to minimize suffering. Mice were maintained on a 12:12-h light/dark cycle with food and water provided ad libitum. Experiments were performed during the light cycle with 13–17 weeks old mice (Fig. S1). *Ncs1*$^{-/-}$ and *Ncs1*$^{+/+}$ mice were generated from heterozygous *Ncs1*$^{+/-}$ breeding pairs, and littermates were used whenever possible.

Displaced object recognition task.

The protocol for the displaced object recognition (DOR) task was based on a previously published protocol (35). DOR experiments were performed in a 35×70×35 cm opaque, white Plexiglas chamber with ~ 1 cm of standard corn cob bedding and captured by a camera mounted above. The testing room was set up with low light conditions (45 Lux). Two 50 ml conical tubes were filled with corn cob bedding and taped – cap-down – to pre-determined positions in the arena. These tubes were selected because mice were unable to climb onto the pointed end of these objects. Approximately 1 h before testing, mice were brought to the testing room and allowed to habituate. For the familiarization phase of the DOR task, each mouse was allowed to explore the arena for 5 min with the two tubes being placed in symmetrical locations. Mice were returned to their cages and 2 h later, they were returned to the arena for another 5 min with one tube remaining in the same position (“familiar”) and 1 tube being moved to a different position (“displaced”). The positions of the tubes were counterbalanced. After each mouse, to remove odor cues, feces were removed, the bedding was shaken, and the tubes were sprayed with 70% ethanol, wiped with tissue paper, sprayed with water, and wiped again. After completion of the experiment, the camera footage was analyzed for bouts of interactions with the tubes. The percent exploration for the displaced object was calculated as [(time spent with displaced object) / (total time spent with both

displaced and familiar objects) * 100] and the percent exploration for the familiar object as [(time spent with familiar object) / (total time spent with both displaced and familiar objects) * 100]. Sniffing and biting were considered to be interactions while casually touching the tubes in passing or leaning onto the tubes to look around were not considered. Data collection and data analysis were performed blinded to the genotype.

Euthanasia and tissue collection.

Each mouse was first anesthetized for ~ 30 s in a chamber with a few drops of 30% isoflurane and then quickly decapitated with sharp scissors. The skull was opened on ice, and the whole brain was extracted and quickly washed in ice-cold 1X phosphate-buffered saline solution (AmericanBio). A razor blade was then used to separate the two hemispheres along the medial longitudinal fissure. Each hemisphere was either immediately dropped into a 25-mL scintillation vial containing 10 mL of impregnation stock solution for Golgi-Cox staining (details below) or rapidly dissected in ice-cold PBS. The isolated hippocampus and frontal cortex were snap-frozen in liquid nitrogen and stored at −80^{o}C until RNA or protein were extracted (details below).

Golgi-Cox staining, imaging, and quantification of neuronal morphology.

Golgi-Cox stock solutions were prepared and staining was performed as previously described (36). Briefly, right after brain extraction, brain hemispheres were impregnated with a potassium dichromate and mercuric chloride solution at room temperature for 7 days. Afterwards, hemispheres were immersed in a cryoprotection solution for 4 days and then sectioned into 200 μm frontal slices with a vibratome. For slice selection, the Golgi Atlas of the Postnatal Mouse Brain was used as a reference to identify the relevant sections in the slices (37). To image the prefrontal cortex (PFC), slices corresponding to frontal sections 4 and 5 were selected. To image the dorsal hippocampus and parietal cortex, slices corresponding to frontal sections 10 and 11 were selected. Selected slices were developed and dehydrated through a series of washing (first increasing alcohol concentrations, then xylene) and drying and finally, mounted in Eukitt solution (Sigma Aldrich) on 0.3% gelatin-coated slides (Thermo Fisher Scientific) for imaging. Z-stack images of the three different brain regions were collected using a Zeiss LSM 710 Duo microscope with 20X objectives to capture whole neurons and 40X objectives to capture individual spines. Neurons that showed intact and complete dendritic arbors, consistent dark staining, and relative isolation from other neurons were selected for imaging. For each mouse and each brain region, 3–4 whole neurons and 6–8 spine segments were captured. The Simple Neurite Tracer plugin for ImageJ (38) was used for analysis. Subsequently, Scholl analysis, quantification of total dendritic length, and quantification of spine density (as the number of spines on dendritic branches per μm dendritic length) were performed.

RNA extraction and sequencing.

RNA was isolated from mouse brain tissues using the RNeasy Mini kit (Qiagen) according to the manufacturer’s protocol. Tissues were homogenized with a polytron and gDNA was removed using gDNA Eliminator columns (Qiagen). The concentration of isolated RNA and total RNA quality were determined using NanoDrop (Thermo Fisher Scientific). RNA integrity was determined with an Agilent Bioanalyzer (2100) which measures the

ratio of ribosomal peaks. Subsequently, samples with a RNA Integrity Number (RIN) ≥ 8 were selected for further experiments. mRNA was purified from approximately 200 ng of total RNA with oligo-dT beads and sheared by incubation at 94 °C in the presence of Mg^{2+} (KAPA mRNA HyperPrep). Following first-strand synthesis with random primers, second-strand synthesis and A-tailing were performed with dUTP for generating strand-specific sequencing libraries. Adapter ligation with 3' dTMP overhangs was ligated to library insert fragments. Library amplification amplified fragments carrying the appropriate adapter sequences at both ends. Strands marked with dUTP were not amplified. Indexed libraries that met appropriate cutoffs for both were quantified through qRT-PCR using a commercially available kit (KAPA Biosystems), and insert size distribution was determined with LabChip GX or Agilent Bioanalyzer. Samples with a yield of at least 0.5 ng/μl were used for sequencing. Sample concentrations were normalized to 1.2 nM and loaded onto an Illumina NovaSeq flow cell at a concentration that yields 25 million passing filter clusters per sample. Samples were sequenced on an Illumina NovaSeq 6000 according to Illumina protocols. The 10bp unique dual index was read during additional sequencing reads that automatically followed the completion of read 1. A positive control (prepared bacteriophage Phi X library) provided by Illumina is spiked into every lane at a concentration of 0.3% to monitor sequencing quality in real time. Signal intensities were converted to individual base calls during a run using the system's Real Time Analysis software. Base calls were transferred from the machine's dedicated personal computer to the Yale High Performance Computing cluster via a 1 Gigabit network mount for downstream analysis.

RNA-Seq analysis.

The RNA-Seq statistical analysis was performed using Partek® Flow® (v 9, 2020 Partek Inc., St. Louis MO, USA). Paired-end reads were aligned to the Genome Reference Consortium Mouse Build 38 (mm10) with the STAR 2.7.3a aligner. Details about the mapping statistics and quality are shown in Table S1. Total counts per gene were quantified with the expectation maximization algorithm and differential gene expression analysis was performed using DESeq2. Subsequently, a list of differentially expressed genes (DEGs) was generated by applying the following filtering criteria: p-value ≤ 0.01 and FC ≥ |1.2| (log2(FC) ≥ |0.26|). Qlucore Omics Explorer 3.6 (Qlucore AB, Lund, Sweden) was used for hierarchical clustering and heatmap generation of $\log_2$ transformed normalized gene expression values (FPKM). For downstream analysis, the Ingenuity Knowledge Base and Ingenuity Pathway Analysis (IPA, v 01–16, QIAGEN Redwood City, USA) were used. Only data that are supported through experimental evidence in the Ingenuity Knowledge Base were considered for analyses. IPA core analysis was performed to identify canonical pathways, diseases, and functions overrepresented in the DEGs and to automatically generate de novo functional networks. The network's score equals the -log(Fisher's Exact test result) based on the hypergeometric distribution of the network.

Database analysis for developmental trajectories.

Evaluation of gene expression trajectories during development was performed using publicly available data sets. Normalized gene expression levels were downloaded from the Kaessmann Lab "Evo-devo mammalian organs" data set (https://apps.kaessmannlab.org/evodevoapp/, (39)) and BrainSpan: Atlas of the Developing Human brain (v10, http://

www.brainspan.org, (40)) on November 3, 2020. Details about data collection and processing are described in the associated publication (39) and the associated white paper (http://help.brain-map.org/display/devhumanbrain/Documentation), respectively. R Statistical Programming Language was used for data transformation and analysis.

Quantitative real-time PCR analysis.

A total of 1 μg RNA was reverse-transcribed to complementary DNA (cDNA) using the High-Capacity cDNA Reverse Transcription Kit according to the manufacturer's protocol (Applied Biosystems). Real-time quantitative PCR (qPCR) was performed in triplicates using Power SYBR Green PCR Master Mix (Applied Biosystems) on a 7500 Fast real-time PCR machine (Applied Biosystems) with primer pairs as listed in Table S2. Fold change in gene expression levels was determined using the ΔΔCt method with 18S as the internal control (41).

Protein extraction and Western blot.0020

Frozen brain samples were transferred into ice-cold radioimmunoprecipitation assay (RIPA) buffer (Santa Cruz) – containing protease inhibitors, phenylmethylsulfonyl fluoride, and sodium orthovanadate –, homogenized with a polytron, and spun down twice for 20 min at 13000 rpm at 4 °C to remove cell debris. Protein concentration was quantified using a bicinchoninic acid assay (Pierce BCA protein assay kit, Thermo Fisher Scientific) according to the manufacturer's instruction. Equal amounts of protein (20 μg per lane) were loaded, and electrophoresis was performed in NuPAGE 4 to 12% gradient Bis-Tris polyacrylamide protein gels (Thermo Fisher Scientific). Transfer was performed using PVDF membranes with the Biorad wet transfer system (Bio-Rad Laboratories). Membranes were blocked with 5% milk in PBS with 0.1% Tween-20 (Sigma Aldrich), incubated overnight with primary antibodies (Table S3) at 4°C, washed, and incubated with secondary antibody for 2 h at room temperature. After a final wash, secondary antibodies were visualized using Pierce ECL chemiluminescence reagents (Thermo Fisher Scientific) and the signal was captured with X-ray films (Thomas Scientific).

Statistical analysis.

Data management and calculations were performed using PRISM Statistical Software 9 (GraphPad Software, Inc, California). Generally, two-tailed student t-test was used to compare two groups and one-way ANOVA followed by Tukey's post-hoc test was used to compare multiple groups. For Sholl analyses, two-way repeated ANOVA followed by Sidak's post-hoc test was used. For statistics on the fold change of gene expressions, a one sample t-test was used. P-values and statistical tests for the individual experiments are reported in detail in the corresponding figure legends. A p-value < 0.05 was considered statistically significant and the following notations were used in all figures: * for $p<0.05$, ** for $p<0.01$, *** for $p<0.001$, and **** for $p<0.0001$. Unless otherwise specified, XY and bar graphs show mean with standard deviation (SD), and box plots show the median, interquartile range, and whiskers ranging from the minimum to maximum value.

Availability of data and materials.

The NGS sequencing data obtained during RNA-Seq studies have been deposited in the Gene Expression Omnibus (GEO) repository by NCBI under the accession number GSE171202. Other data needed to evaluate this paper's conclusions are provided within the manuscript and the supplementary information. Laboratory protocols are described and cited in Material and Methods. Further information is available upon request from the corresponding author.

Results

To better understand the role of NCS1 in neuronal functions, wildtype (WT, *Ncs1*$^{+/+}$) and homozygous *Ncs1* whole-body knockout (KO, *Ncs1*$^{-/-}$) mice were examined in a three-stage experimental setup containing behavioral, neuro-morphological, and molecular assessments (Fig. 1A). We focused on the frontal cortex and the hippocampus because previous studies indicate a particularly important role for NCS1-dependent signaling in these brain regions (14, 15, 18, 21).

Confirmation of the *Ncs1*$^{-/-}$ mouse model

Using RNA-Seq, we confirmed the deletion of exons 4–7 of *Ncs1* in the frontal cortex and the hippocampus of constitutive *Ncs1*$^{-/-}$ mice generated previously (Fig. 1B–C) (33, 34). Immunoblotting with a polyclonal antibody indicated the complete loss of NCS1 protein in these *Ncs1*$^{-/-}$ tissues (Fig. 1D). The displaced object recognition (DOR) task revealed deficits in spatial memory acquisition in *Ncs1*$^{-/-}$ mice (Fig. 1E, *Ncs1*$^{+/+}$: p=0.0009, *Ncs1*$^{-/-}$: p=0.65), which indicates impaired cortical and hippocampal functionality (42, 43), recapitulating results from previous studies in *Ncs1*$^{-/-}$ mice (15, 21).

Ncs1$^{-/-}$ mice show reduced neuronal complexity and spine density in the prefrontal cortex

To investigate underlying cellular correlates of the impaired performance of *Ncs1*$^{-/-}$ mice in the DOR task, Golgi-Cox staining on brain hemispheres from *Ncs1*$^{+/+}$ and *Ncs1*$^{-/-}$ mice, followed by Sholl analysis and spine quantification, was performed. First, we investigated layer II/III pyramidal neurons in the prefrontal cortex (PFC) (Fig. 2A–B). Sholl analysis revealed that basal dendrites in *Ncs1*$^{-/-}$ mice exhibit a significantly reduced complexity in dendritic arborization (Fig. 2C, p=0.005), with a significant interaction between genotype and distance from the cell soma (p<0.0001). Post-hoc analysis revealed that a reduction of dendritic intersections occurred particularly between 20–60 μm from the cell soma. These deficits in complexity were associated with a 26% reduction in total basal dendritic length in *Ncs1*$^{-/-}$ mice (Fig. 2D, p=0.001). Moreover, basal dendrites of layer II/III pyramidal neurons in the PFC of *Ncs1*$^{-/-}$ mice showed a 14% reduction in spine density (Fig. 2E–F, p=0.0005). In contrast, for apical dendrites, no significant differences in dendritic complexity (Fig. 2G, p=0.96), total dendritic length (Fig. 2H, p=0.35), or spine density (Fig. 2I–J, p=0.11) were observed between the two groups.

Analysis of layer II/III cortical pyramidal neurons in the parietal cortex revealed no alterations of basal or apical dendrites in *Ncs1*$^{-/-}$ mice (Fig. S2). These results suggest

that the loss of *Ncs1* results in region-specific impairments of neuronal morphology in the PFC, whereas morphology in the parietal cortex is not altered.

Ncs1$^{-/-}$ mice show reduced neuronal complexity and spine density in the dorsal hippocampus

Neuronal morphology was also assessed in the dorsal hippocampus, specifically in granule cells of the dentate gyrus (Fig. 3A–B). We found that granule cells from *Ncs1*$^{-/-}$ mice show a significant reduction in the complexity of dendritic arborization (Fig. 3C, p=0.0012), with a significant interaction between genotype and distance from the cell soma (p<0.0001). Particularly, dendritic intersections were reduced between 70–150 μm from the cell soma. In addition, *Ncs1*$^{-/-}$ granule cells showed a 31% reduction in total dendritic length (Fig. 2D, p=0.0002) and a 10% reduction in spine density (Fig. 2E–F, p=0.011).

RNA-Seq transcriptome analysis in the frontal cortex and hippocampus of *Ncs1*$^{+/+}$ and *Ncs1*$^{-/-}$ mice

To provide insights into the effects of *Ncs1*$^{-/-}$ on gene expression patterns potentially contributing to the *Ncs1*$^{-/-}$ phenotype, we performed bulk whole-transcriptome RNA-Seq of the frontal cortex and the hippocampus of *Ncs1*$^{+/+}$ and *Ncs1*$^{-/-}$ mice using Illumina next-generation sequencing (Table S1). Fig. 4A–B shows the results of the differential gene expression analysis comparing *Ncs1*$^{-/-}$ with *Ncs1*$^{+/+}$ samples for all ~17,000 genes in the frontal cortex and the hippocampus. Mild but distinct transcriptional changes were observed in both regions. By applying filtering criteria ($p < 0.01$, fold change $\geq |1.2|$), lists of differentially expressed genes (DEGs) were generated (Fig. 4E, Table S4, S5). In the frontal cortex of *Ncs1*$^{-/-}$ mice, 267 DEGs were identified, with 47 genes being down- and 220 genes being upregulated. In the hippocampus of *Ncs1*$^{-/-}$ mice, 74 DEGs were identified, with 14 genes being down- and 60 genes being upregulated. Based on $\log_2$-transformed normalized gene expression values of the DEGs, unsupervised hierarchical clustering revealed that samples with the same underlying genotype clustered together and that non-random gene expression patterns can be identified in *Ncs1*$^{-/-}$ brain tissue (Fig. 4C–D). Subsequently, top hits and DEGs with particular biological significance were validated in the frontal cortex and the hippocampus using real-time quantitative-PCR (qPCR) (Fig. 4F). Samples used for RNA-Seq experiments and samples from another 6 mice per genotype were used for both technical and biological validation. Whereas in the RNA-Seq experiments, *Rock1* and *Dcx* only passed the cutoffs for a DEG in the frontal cortex (Hippocampus: *Rock1*: p=0.01, FC=1.16; *Dcx*: p=0.18, FC=1.1), their upregulation was consistent across frontal cortex and hippocampus in the qPCR experiments.

NCS1 modulates cell morphology, neurological diseases, and development at the transcriptional level

After determining that NCS1 affects gene expression, we leveraged the Ingenuity Knowledge Base for systems biology analysis of our RNA-Seq results. Tables 1 and 2 show the top 5 significantly enriched processes in the “molecular and cellular functions,” “diseases and disorders,” and “physiological system development and function” categories. The top 5 and top 3 differentially regulated molecular and cellular functions in the frontal cortex and the hippocampus, respectively, are related to cellular structure and development

(Table 1A, 2A). Consistent with altered structural functionality, pathways that are enriched in the frontal cortex include endocytosis, actin cytoskeleton signaling, rho signaling, cell junction signaling, and Ca2+ signaling (Table S6). In the hippocampus, differentially regulated pathways include senescence signaling, rank signaling, and amyotrophic lateral sclerosis signaling (Table S7). Because aberrant expression or functioning of NCS1 was previously implicated in the pathophysiology of several neurological and neurodevelopmental diseases (7, 22–31), it was notable that in our unbiased systems analysis, NCS1-mediated gene regulation appears to be linked to neurological diseases and developmental processes - both in the frontal cortex and hippocampus (Table 1B–C, 2B–C).

Next, de novo automated network generation with DEGs identified in *Ncs1*$^{-/-}$ mice was performed using the Ingenuity Pathway Analysis (IPA) algorithm (Table S8–9). Fig. 5A–B depicts the networks “Developmental disorder, neurological disease, organismal injury and abnormalities” and “Developmental disorder, hereditary disorder, neurological disease” for the frontal cortex and hippocampus, respectively. These networks support that *Ncs1*-mediated gene transcription patterns are involved in neurological disease and development. The Ingenuity Knowledge Base did not report any direct interactions between NCS1 and the two networks but identified several intermediate molecules such as Ca2+, DRD2, ITPR1, cAMP, and MAPK1. Particularly, through Ca2+, *NCS1* regulates several nodes in the cortical and hippocampal networks.

NCS1 transcript levels increase during prenatal brain development and regulate RhoA/ROCK1/LIMK/cofilin signaling

The enrichment analysis of the DEGs identified in *Ncs1*$^{-/-}$ mice and the relatively young age at which these mice showed behavioral and neuro-morphological impairments suggest deficits in neurodevelopment. Therefore, we retrieved developmental gene expression data from early organogenesis to middle adulthood from two publicly available data sets (https://apps.kaessmannlab.org/evodevoapp/, http://www.brainspan.org). The Kaessmann Lab data set provides gene expression data in the forebrain for several species (human, macaque, mouse, rat, opossum, and chicken). In mice and humans, we identified a distinct pattern of *Ncs1* gene expression with a significant increase during prenatal brain development when neuronal proliferation, migration, and maturation occur. This increase is followed by a relative plateau during the postnatal period (Fig. 6A–B, mouse: R^2=0.91, human: R^2=0.71, Fig. S3E). This trajectory was observed similarly in the other four species, indicating evolutionary conservation (Fig. S3A–E). Subsequent investigation of different human brain regions using the BrainSpan data set revealed a similar trajectory of *NCS1* gene expression in the neocortex and the hippocampus with a significant increase during the first two trimesters (Fig. 6C–D, neocortex: R^2=0.41, hippocampus: R^2=0.64, Fig. S3F). Exploring other available brain regions, we observed a later increase in *NCS1* gene expression in the amygdala, whereas the cerebellum, thalamus, and striatum showed no clear trend, suggesting region-specific *NCS1* trajectories (Fig. S3F–J). Using a previously published approach (44), we then evaluated transcriptional co-expression between *NCS1* and each DEG identified in our RNA-Seq experiments by calculating Pearson’s correlation coefficient over 8 developmental stages. We found a strong correlation (Pearson’s $r \geq |0.7|$) for 52 DEGs in the frontal cortex and 19 DEGs in the hippocampus (Fig. 6E–F). Notably, *ROCK1*

was negatively correlated with *NCS1* during development, *Rock1* was upregulated both in the frontal cortex and the hippocampus of *Ncs1*$^{-/-}$ mice (Fig. 4F), and Rock1 was part of the significantly activated pathway “Signaling of Rho Family GTPases” (Table S6) and the cortical network in *Ncs1*$^{-/-}$ mice (Fig. 5A). Subsequent immunoblotting revealed a strong increase in the phosphorylation levels – hence inhibition – of cofilin, a downstream target of the RhoA/ROCK1/LIMK signaling axis and a key regulator of neuronal morphology (45, 46), in the frontal cortex and hippocampus of 4 out of 5 *Ncs1*$^{-/-}$ mice (Fig. 6G–H).

Discussion

Here, we investigated the function of NCS1 in the brain at the molecular, cellular, and organismal levels and report novel insights into NCS1-dependent signaling and its downstream effects. We found that NCS1 modulates gene expression, dendritic morphology, and cognitive functions, particularly in a region-specific manner. Combined with further analysis of developmental databases, our results support a significant role of NCS1 in neurodevelopment.

NCS1 as a modulator of gene expression

Although Ca2+ signaling is a well-established and versatile regulator of gene transcription (47, 48), a role for NCS1 in this process has only recently been suggested in dopaminergic neurons and cardiomyocytes (9, 49). Here, we performed, to our knowledge, RNA-Seq of *Ncs1*$^{-/-}$ mouse tissues for the first time. Our analysis revealed mild and region-specific differential gene expression in the frontal cortex and the hippocampus of *Ncs1*$^{-/-}$ compared with *Ncs1*$^{+/+}$ mice. Systems biology analysis indicated that NCS1 affects transcriptomics of a broad range of signaling pathways, particularly related to cell morphology and neurodevelopment, which may explain the results we obtained from Golgi-Cox experiments and stimulated further analysis of developmental databases. A subtle but broad regulatory effect of NCS1 on gene expression was expected – and filtering criteria for the differential gene expression analysis were set accordingly – because NCS1 is not a direct transcription factor but can affect gene expression indirectly through its role in regulating cytosolic and nuclear Ca2+ signals (9–11, 50). For example, previous studies suggest that NCS1 is involved in the cytosolic activation of Ca2+/CaM-dependent protein kinase CaMKII, which is a major regulator of transcription factors like cAMP response element-binding protein CREB (21, 51, 52). Similarly, it has been reported that hippocalcin, another member of the neuronal Ca2+ sensor family, regulates CREB (53).

Our data did not suggest transcriptional compensation in *Ncs1*$^{-/-}$ mice via any of the other members of the EF-Hand Ca2+ sensor family (6). Notably, *Ncs1*$^{-/-}$ tissues also did not show alterations in the gene expression of major Ca2+ channels except for a mild upregulation of *Cacna1e* ($Ca_V2.3$) in the frontal cortex and *Cacna1d* ($Ca_V1.3$) in the hippocampus. Previous studies implicated a downregulation of *Cacna1e* in *Ncs1*-deficient substantia nigra dopaminergic neurons in Parkinson’s disease (25, 49), further supporting the notion of region-specific NCS1-dependent gene expression.

NCS1 in the regulation of neuronal morphology

The enrichment of morphology-related processes in our RNA-Seq data set is consistent with the neuro-morphological impairments that we observed in *Ncs1*$^{-/-}$ mice. Particularly, our systems biology analysis pointed to a novel connection between NCS1 and Actin/Rho signaling, specifically the Rock/LIMK/Cofilin pathway, a crucial effector in the spatiotemporal regulation of neuronal morphology (54). Intact cofilin dynamics are critical for morphology, particularly neurite outgrowth and synaptic plasticity underlying long-term potentiation (LTP) and depression (LTD) (45, 46). Therefore, upregulation of *Rock1* and hyperphosphorylation, hence inactivation, of cofilin may contribute to impaired dendritic functioning in *Ncs1*$^{-/-}$ mice. Furthermore, as the activity of this pathway is Ca2+ sensitive, NCS1 may regulate Rho signaling both at the transcriptional and post-translational levels (55, 56).

A role for NCS1 in regulating neuronal morphology is supported by previous studies describing that NCS1 enhances neurite outgrowth (16–18) and synaptic transmission, specifically neurotransmitter release, LTP, and LTD (12–15). Similarly, NCS1 regulates exocytosis in adrenal chromaffin cells (57), morphology of cardiomyocytes (52), and motility of cancer cells (50, 58). The gross morphology of the brain has been reported to be unaltered in *Ncs1*$^{-/-}$ mice (21). Reduced dendritic morphology in *Ncs1*$^{-/-}$ mice may be due to several, not mutually exclusive mechanisms. As neuronal morphology and neuronal activity are intertwined phenomena, one mechanism may be deficits in activity-dependent neuronal maturation and neuroplasticity. Given the embryonic deletion of NCS1 in the current mouse model and our results pointing to a molecular role of NCS1 in neurodevelopment, another mechanism may involve morphological deficits in the early stages of development, preceding deficits in maturation.

At the organismal level, impaired dendritic morphology in the PFC, including the medial prefrontal cortex (mPFC), and the dorsal hippocampus – regions critical for spatial memory acquisition (42) – is a likely correlate for the cognitive deficits observed in *Ncs1*$^{-/-}$ mice. Unaltered morphology in the parietal cortex, on the other hand, is consistent with our previous observation that *Ncs1*$^{-/-}$ mice showed minimal differences in somatosensory and motor functions (59). A specificity of NCS1-dependent effects for certain brain regions, cell types, and subcellular areas, is highlighted throughout the NCS1 literature and may be due to specific *NCS1* expression patterns, differential availability of its target proteins, and different neuronal Ca2+ signals (7, 12). This phenomenon can also explain why a different study described a mild increase in total dendritic complexity without significant changes in spine density in the frontal cortex of *Ncs1*$^{-/-}$ mice (15). The importance yet complexity of NCS1-dependent modulation of spines is emphasized by the observation that some NCS1-associated neurodevelopmental and psychiatric diseases show increased spine density, such as ASD, whereas others show reduced spine density, such as bipolar disorder and schizophrenia (60). Notably, pharmacological targeting of the complex between NCS1 and the guanine exchange factor protein Ric8a (Synembryn-A) can rescue both types of synaptopathies *in vivo* (23, 26).

A molecular role for NCS1 in early brain development and neurodevelopmental diseases

During fetal brain development, precise Ca2+ signals are necessary for the spatiotemporal regulation of neuronal proliferation, migration, and differentiation, which requires, for example, temporal gene expression patterns of Ca2+ channels (2). Here, we identified across several species a distinct temporal expression pattern of *NCS1* in the forebrain, particularly the frontal cortex and hippocampus. Several DEGs identified in the frontal cortex and the hippocampus in our RNA-Seq experiments showed a significant correlation with the *NCS1* developmental trajectory, supporting biologically relevant functions of NCS1 in brain development. For example, *NCS1* and *ROCK1* showed a strong negative correlation, which may underly NCS1-dependent effects on neuronal morphology as discussed above. Previous studies also implicated NCS1 in the development of the retina (61), olfactory bulb (62), and spinal cord (63). As most of the other Ca2+ sensor proteins also show distinct temporal trajectories (Fig. S4), we hypothesize that temporal expression patterns of Ca2+ sensors are critical for the finetuning of neurodevelopmental processes, including electrophysiological, morphological, and transcriptional changes. The importance of precisely regulated trajectories of *NCS1* expression may explain why, for example, abnormal increases in *NCS1* expression have been linked to bipolar disorder and schizophrenia (30).

Limitations and future directions

Investigating the effect of abnormal *NCS1* expression or the R102Q NCS1 mutant, identified in a case of ASD (22), on developmental signaling and neuronal morphology will further improve the understanding of NCS1-related disease mechanisms. To validate a molecular function of NCS1 during development, an assessment of *Ncs1*$^{-/-}$ mice at different developmental time points or conditional knockout of *Ncs1* at different developmental stages will be necessary. Future molecular, morphological, and functional assays will elucidate the specific stages of neurodevelopment – including neurogenesis, differentiation, migration, and maturation – where alterations in the brain of *Ncs1*$^{-/-}$ mice first occur. Region-specific NCS1-dependent effects highlighted in this study will stimulate assessments of multiple brain regions and subregions in *Ncs1*$^{-/-}$ mice in further detail, particularly including, for example, the mPFC, dentate gyrus, and CA1/3 in the context of the memory deficits observed in *Ncs1*$^{-/-}$ mice. Furthermore, for morphological analyses, a comparison between the effect of NCS1 on axonal and dendritic growth will facilitate a better understanding of NCS1 functions on a subcellular level. For example, at the molecular level, the relationship between NCS1 and DCX, a DEG identified in this study and a known marker for neurogenesis in development and adulthood (64), should be investigated during development.

A role of NCS1 in development should also be considered in other organs and the whole organism because one study reported decreased survival of *Ncs1*$^{-/-}$ pups (52), whereas others did not observe this effect (65). Sex-specific differences of *Ncs1*$^{-/-}$ mice are also important to keep in mind (59). Furthermore, as this study suggests that precise *NCS1* expression levels are critical for neurodevelopment and previous studies described an association between increased *NCS1* expression and patient survival in liver and breast

cancer (66–68), we suggest evaluating the predictive capacity of *NCS1* expression in neurooncological cohorts as well.

The main limitations of our RNA-Seq experiments are that the cohort size was small compared to the effect size, and whole tissue transcriptome analysis only provides limited insights into neuron-specific signaling. Future studies will uncover the effect of NCS1 in different cell types and regions of the CNS, for example, through single-cell RNA-Seq, and determine the mechanisms underlying NCS1-dependent neuronal gene expression. Overall, an improved understanding of NCS1-dependent signaling will inform drug development studies targeting NCS1 and its protein interactions, such as a recently developed NCS1-directed dynamic combinatorial chemistry approach for the treatment of synaptopathies (26) or drug repurposing studies targeting NCS1 for the treatment of Wolfram syndrome (27).

Conclusions

Using RNA-Sequencing, Golgi-Cox staining, behavioral experiments, and data-mining strategies, we provide novel insights into the diverse functions of NCS1 in the brain. Specifically, our results suggest that NCS1-dependent gene expression patterns in the frontal cortex and the hippocampus contribute to the impairments in neuronal morphology and memory acquisition concomitantly observed in these mice. Furthermore, we propose that NCS1 is a novel modulator of Ca2+-dependent, spatiotemporal processes during early brain development. This study lays the foundation for future investigations of NCS1 in neurodevelopmental processes with implications for the understanding of and drug development for neurodevelopmental and neuropsychiatric diseases.

Supplementary Material

Refer to Web version on PubMed Central for supplementary material.

Acknowledgments

We thank the Yale Center for Genomic Analysis (YCGA) for their assistance with RNA-Sequencing experiments. We thank Nur-Taz Rahman and Rolando Garcia Milan (Yale Medical Library Bioinformatics Support Program) and Vladimir Kuryshev (Institute of Pharmacology, University Hospital Heidelberg, Germany) for their help with the bioinformatics analyses. We thank Sravan Perla, Jae-Sung Yi, and Lei Zhang (Department of Pharmacology, Yale University) for technical support and critical discussions. We thank Marc Freichel (Institute of Pharmacology, University Hospital Heidelberg, Germany) for great mentorship and helpful discussions. We thank Paulina Schad (University of Heidelberg, Germany) and Daniel Schütte (University of Cologne, Germany) for thoughtful comments on the manuscript.

Funding.

NIH grant 5P01DK057751 and a gift from a generous donor (B.E.E) supported this work. T.T.F. was supported by a scholarship from the German Academic Scholarship Foundation

Nonstandard abbreviations

ASD	Autism Spectrum Disorder
Ca2+	Calcium
Cacna1d	Calcium Voltage-Gated Channel Subunit Alpha1 D

Cacna1e	Calcium Voltage-Gated Channel Subunit Alpha1 E
CaM	Calmodulin
CaMKII	Calcium/calmodulin-dependent protein kinase II
cAMP	cyclic adenosine monophosphate
Ca_v	Voltage gated calcium channels
Cercam	Cerebral Endothelial Cell Adhesion Molecule
CREB	cAMP response element-binding protein
Dcx	Doublecortin
DEG	Differentially expressed gene
DOR	Displaces object recognition
D2R	Dopamine receptor D2
Frq	Frequenin
FXS	Fragile X syndrome
Hmcn2	Hemicentin 2
HTT	Huntingtin
InsP3R	Inositol 1,4,5-Trisphosphate Receptor
ITPR1	Inositol 1,4,5-Trisphosphate Receptor Type 1
LIMK	LIM domain kinase 1
LTD	Long term depression
LTP	Long term potentiation
Lypd6b	Ly6/PLAUR Domain-Containing Protein 6B
MAPK1	Mitogen-activated protein kinase 1
MYOC	Myocilin
NCS1	Neuronal calcium sensor 1
$Ncs1^{-/-}$	Neuronal calcium sensor 1 knockout
$Ncs1^{+/+}$	Neuronal calcium sensor 1 wildtype
PFC	Prefrontal cortex
Rbm43	RNA Binding Motif Protein 43
RhoA	Ras Homolog Family Member A

Ric8a	RIC8 Guanine Nucleotide Exchange Factor A
RNA-Seq	RNA-Sequencing
Rock1	Rho Associated Coiled-Coil Containing Protein Kinase 1
SPP1	Secreted Phosphoprotein 1
Thbs1	Thrombospondin 1
TRAF2	TNF Receptor Associated Factor 2
Trub2	TruB Pseudouridine Synthase Family Member 2

References

1. Brini M, Cali T, Ottolini D, and Carafoli E (2014) Neuronal calcium signaling: function and dysfunction. Cell Mol Life Sci 71, 2787–2814 [PubMed: 24442513]
2. Toth AB, Shum AK, and Prakriya M (2016) Regulation of neurogenesis by calcium signaling. Cell Calcium 59, 124–134 [PubMed: 27020657]
3. Bezprozvanny I (2009) Calcium signaling and neurodegenerative diseases. Trends Mol Med 15, 89–100 [PubMed: 19230774]
4. Berridge MJ (2014) Calcium signalling and psychiatric disease: bipolar disorder and schizophrenia. Cell Tissue Res 357, 477–492 [PubMed: 24577622]
5. Nguyen RL, Medvedeva YV, Ayyagari TE, Schmunk G, and Gargus JJ (2018) Intracellular calcium dysregulation in autism spectrum disorder: An analysis of converging organelle signaling pathways. Biochim Biophys Acta Mol Cell Res 1865, 1718–1732 [PubMed: 30992134]
6. Mikhaylova M, Hradsky J, and Kreutz MR (2011) Between promiscuity and specificity: novel roles of EF-hand calcium sensors in neuronal Ca2+ signalling. J Neurochem 118, 695–713 [PubMed: 21722133]
7. Bandura J, and Feng ZP (2019) Current Understanding of the Role of Neuronal Calcium Sensor 1 in Neurological Disorders. Mol Neurobiol 56, 6080–6094 [PubMed: 30719643]
8. Pongs O, Lindemeier J, Zhu XR, Theil T, Engelkamp D, Krah-Jentgens I, Lambrecht HG, Koch KW, Schwemer J, Rivosecchi R, and et al. (1993) Frequenin--a novel calcium-binding protein that modulates synaptic efficacy in the Drosophila nervous system. Neuron 11, 15–28 [PubMed: 8101711]
9. Nakao S, Wakabayashi S, and Nakamura TY (2015) Stimulus-dependent regulation of nuclear Ca2+ signaling in cardiomyocytes: a role of neuronal calcium sensor-1. PLoS One 10, e0125050 [PubMed: 25897502]
10. Nakamura TY, Nakao S, and Wakabayashi S (2019) Emerging Roles of Neuronal Ca(2+) Sensor-1 in Cardiac and Neuronal Tissues: A Mini Review. Front Mol Neurosci 12, 56 [PubMed: 30886571]
11. Nguyen LD, Petri ET, Huynh LK, and Ehrlich BE (2019) Characterization of NCS1-InsP3R1 interaction and its functional significance. J Biol Chem 294, 18923–18933 [PubMed: 31659121]
12. Dason JS, Romero-Pozuelo J, Atwood HL, and Ferrus A (2012) Multiple roles for frequenin/NCS-1 in synaptic function and development. Mol Neurobiol 45, 388–402 [PubMed: 22396213]
13. Tsujimoto T, Jeromin A, Saitoh N, Roder JC, and Takahashi T (2002) Neuronal calcium sensor 1 and activity-dependent facilitation of P/Q-type calcium currents at presynaptic nerve terminals. Science 295, 2276–2279 [PubMed: 11910115]
14. Saab BJ, Georgiou J, Nath A, Lee FJ, Wang M, Michalon A, Liu F, Mansuy IM, and Roder JC (2009) NCS-1 in the dentate gyrus promotes exploration, synaptic plasticity, and rapid acquisition of spatial memory. Neuron 63, 643–656 [PubMed: 19755107]

15. Ng E, Georgiou J, Avila A, Trought K, Mun HS, Hodgson M, Servinis P, Roder JC, Collingridge GL, and Wong AHC (2020) Mice lacking neuronal calcium sensor-1 show social and cognitive deficits. Behav Brain Res 381, 112420 [PubMed: 31821787]

16. Hui K, Fei GH, Saab BJ, Su J, Roder JC, and Feng ZP (2007) Neuronal calcium sensor-1 modulation of optimal calcium level for neurite outgrowth. Development 134, 4479–4489 [PubMed: 18039973]

17. Iketani M, Imaizumi C, Nakamura F, Jeromin A, Mikoshiba K, Goshima Y, and Takei K (2009) Regulation of neurite outgrowth mediated by neuronal calcium sensor-1 and inositol 1,4,5-trisphosphate receptor in nerve growth cones. Neuroscience 161, 743–752 [PubMed: 19368896]

18. Yip PK, Wong LF, Sears TA, Yanez-Munoz RJ, and McMahon SB (2010) Cortical overexpression of neuronal calcium sensor-1 induces functional plasticity in spinal cord following unilateral pyramidal tract injury in rat. PLoS Biol 8, e1000399 [PubMed: 20585375]

19. Nakamura TY, Jeromin A, Smith G, Kurushima H, Koga H, Nakabeppu Y, Wakabayashi S, and Nabekura J (2006) Novel role of neuronal Ca2+ sensor-1 as a survival factor up-regulated in injured neurons. J Cell Biol 172, 1081–1091 [PubMed: 16549499]

20. Gomez M, De Castro E, Guarin E, Sasakura H, Kuhara A, Mori I, Bartfai T, Bargmann CI, and Nef P (2001) Ca2+ signaling via the neuronal calcium sensor-1 regulates associative learning and memory in C. elegans. Neuron 30, 241–248 [PubMed: 11343658]

21. Nakamura TY, Nakao S, Nakajo Y, Takahashi JC, Wakabayashi S, and Yanamoto H (2017) Possible Signaling Pathways Mediating Neuronal Calcium Sensor-1-Dependent Spatial Learning and Memory in Mice. PLoS One 12, e0170829 [PubMed: 28122057]

22. Handley MT, Lian LY, Haynes LP, and Burgoyne RD (2010) Structural and functional deficits in a neuronal calcium sensor-1 mutant identified in a case of autistic spectrum disorder. PLoS One 5, e10534 [PubMed: 20479890]

23. Mansilla A, Chaves-Sanjuan A, Campillo NE, Semelidou O, Martinez-Gonzalez L, Infantes L, Gonzalez-Rubio JM, Gil C, Conde S, Skoulakis EM, Ferrus A, Martinez A, and Sanchez-Barrena MJ (2017) Interference of the complex between NCS-1 and Ric8a with phenothiazines regulates synaptic function and is an approach for fragile X syndrome. Proc Natl Acad Sci U S A 114, E999–E1008 [PubMed: 28119500]

24. Dragicevic E, Poetschke C, Duda J, Schlaudraff F, Lammel S, Schiemann J, Fauler M, Hetzel A, Watanabe M, Lujan R, Malenka RC, Striessnig J, and Liss B (2014) Cav1.3 channels control D2-autoreceptor responses via NCS-1 in substantia nigra dopamine neurons. Brain 137, 2287–2302 [PubMed: 24934288]

25. Benkert J, Hess S, Roy S, Beccano-Kelly D, Wiederspohn N, Duda J, Simons C, Patil K, Gaifullina A, Mannal N, Dragicevic E, Spaich D, Muller S, Nemeth J, Hollmann H, Deuter N, Mousba Y, Kubisch C, Poetschke C, Striessnig J, Pongs O, Schneider T, Wade-Martins R, Patel S, Parlato R, Frank T, Kloppenburg P, and Liss B (2019) Cav2.3 channels contribute to dopaminergic neuron loss in a model of Parkinson's disease. Nat Commun 10, 5094 [PubMed: 31704946]

26. Canal-Martin A, Sastre J, Sanchez-Barrena MJ, Canales A, Baldominos S, Pascual N, Martinez-Gonzalez L, Molero D, Fernandez-Valle ME, Saez E, Blanco-Gabella P, Gomez-Rubio E, Martin-Santamaria S, Saiz A, Mansilla A, Canada FJ, Jimenez-Barbero J, Martinez A, and Perez-Fernandez R (2019) Insights into real-time chemical processes in a calcium sensor protein-directed dynamic library. Nat Commun 10, 2798 [PubMed: 31243268]

27. Nguyen LD, Fischer TT, Abreu D, Arroyo A, Urano F, and Ehrlich BE (2020) Calpain inhibitor and ibudilast rescue beta cell functions in a cellular model of Wolfram syndrome. Proc Natl Acad Sci U S A 117, 17389–17398 [PubMed: 32632005]

28. Fischer TT, and Ehrlich BE (2020) Wolfram Syndrome: a Monogenic Model to Study Diabetes Mellitus and Neurodegeneration. Curr Opin Physiol 17, 115–123 [PubMed: 32864536]

29. Angebault C, Fauconnier J, Patergnani S, Rieusset J, Danese A, Affortit CA, Jagodzinska J, Megy C, Quiles M, Cazevieille C, Korchagina J, Bonnet-Wersinger D, Milea D, Hamel C, Pinton P, Thiry M, Lacampagne A, Delprat B, and Delettre C (2018) ER-mitochondria cross-talk is regulated by the Ca(2+) sensor NCS1 and is impaired in Wolfram syndrome. Sci Signal 11

30. Koh PO, Undie AS, Kabbani N, Levenson R, Goldman-Rakic PS, and Lidow MS (2003) Up-regulation of neuronal calcium sensor-1 (NCS-1) in the prefrontal cortex of schizophrenic and bipolar patients. Proc Natl Acad Sci U S A 100, 313–317 [PubMed: 12496348]

31. Torres KC, Souza BR, Miranda DM, Sampaio AM, Nicolato R, Neves FS, Barros AG, Dutra WO, Gollob KJ, Correa H, and Romano-Silva MA (2009) Expression of neuronal calcium sensor-1 (NCS-1) is decreased in leukocytes of schizophrenia and bipolar disorder patients. Prog Neuropsychopharmacol Biol Psychiatry 33, 229–234 [PubMed: 19091302]
32. Schlecker C, Boehmerle W, Jeromin A, DeGray B, Varshney A, Sharma Y, Szigeti-Buck K, and Ehrlich BE (2006) Neuronal calcium sensor-1 enhancement of InsP3 receptor activity is inhibited by therapeutic levels of lithium. J Clin Invest 116, 1668–1674 [PubMed: 16691292]
33. Hermainski JG (2012) Untersuchungen zur Funktion des Neuronalen Calcium Sensors 1 (NCS-1) an genetisch veränderten Mauslinien (Mus musculus, Linnaeus 1758). Verlag Dr. Hut
34. Ng E, Varaschin RK, Su P, Browne CJ, Hermainski J, Le Foll B, Pongs O, Liu F, Trudeau LE, Roder JC, and Wong AH (2016) Neuronal calcium sensor-1 deletion in the mouse decreases motivation and dopamine release in the nucleus accumbens. Behav Brain Res 301, 213–225 [PubMed: 26738968]
35. Vogel-Ciernia A, and Wood MA (2014) Examining object location and object recognition memory in mice. Curr Protoc Neurosci 69, 8 31 31–17 [PubMed: 25297693]
36. Nguyen LD, Fischer TT, and Ehrlich BE (2021) Pharmacological rescue of cognitive function in a mouse model of chemobrain. Mol Neurodegener 16, 41 [PubMed: 34174909]
37. Valverde F (1998) Golgi Atlas of the Postnatal Mouse Brain. Springer, Vienna
38. Longair MH, Baker DA, and Armstrong JD (2011) Simple Neurite Tracer: open source software for reconstruction, visualization and analysis of neuronal processes. Bioinformatics 27, 2453–2454 [PubMed: 21727141]
39. Cardoso-Moreira M, Halbert J, Valloton D, Velten B, Chen C, Shao Y, Liechti A, Ascencao K, Rummel C, Ovchinnikova S, Mazin PV, Xenarios I, Harshman K, Mort M, Cooper DN, Sandi C, Soares MJ, Ferreira PG, Afonso S, Carneiro M, Turner JMA, VandeBerg JL, Fallahshahroudi A, Jensen P, Behr R, Lisgo S, Lindsay S, Khaitovich P, Huber W, Baker J, Anders S, Zhang YE, and Kaessmann H (2019) Gene expression across mammalian organ development. Nature 571, 505–509 [PubMed: 31243369]
40. Miller JA, Ding SL, Sunkin SM, Smith KA, Ng L, Szafer A, Ebbert A, Riley ZL, Royall JJ, Aiona K, Arnold JM, Bennet C, Bertagnolli D, Brouner K, Butler S, Caldejon S, Carey A, Cuhaciyan C, Dalley RA, Dee N, Dolbeare TA, Facer BA, Feng D, Fliss TP, Gee G, Goldy J, Gourley L, Gregor BW, Gu G, Howard RE, Jochim JM, Kuan CL, Lau C, Lee CK, Lee F, Lemon TA, Lesnar P, McMurray B, Mastan N, Mosqueda N, Naluai-Cecchini T, Ngo NK, Nyhus J, Oldre A, Olson E, Parente J, Parker PD, Parry SE, Stevens A, Pletikos M, Reding M, Roll K, Sandman D, Sarreal M, Shapouri S, Shapovalova NV, Shen EH, Sjoquist N, Slaughterbeck CR, Smith M, Sodt AJ, Williams D, Zollei L, Fischl B, Gerstein MB, Geschwind DH, Glass IA, Hawrylycz MJ, Hevner RF, Huang H, Jones AR, Knowles JA, Levitt P, Phillips JW, Sestan N, Wohnoutka P, Dang C, Bernard A, Hohmann JG, and Lein ES (2014) Transcriptional landscape of the prenatal human brain. Nature 508, 199–206 [PubMed: 24695229]
41. Wieckowski MR, Giorgi C, Lebiedzinska M, Duszynski J, and Pinton P (2009) Isolation of mitochondria-associated membranes and mitochondria from animal tissues and cells. Nat Protoc 4, 1582–1590 [PubMed: 19816421]
42. DeVito LM, and Eichenbaum H (2010) Distinct contributions of the hippocampus and medial prefrontal cortex to the “what-where-when” components of episodic-like memory in mice. Behav Brain Res 215, 318–325 [PubMed: 19766146]
43. Antunes M, and Biala G (2012) The novel object recognition memory: neurobiology, test procedure, and its modifications. Cogn Process 13, 93–110 [PubMed: 22160349]
44. Gulsuner S, Walsh T, Watts AC, Lee MK, Thornton AM, Casadei S, Rippey C, Shahin H, Consortium on the Genetics of S, Group PS, Nimgaonkar VL, Go RC, Savage RM, Swerdlow NR, Gur RE, Braff DL, King MC, and McClellan JM (2013) Spatial and temporal mapping of de novo mutations in schizophrenia to a fetal prefrontal cortical network. Cell 154, 518–529 [PubMed: 23911319]
45. Flynn KC, Hellal F, Neukirchen D, Jacob S, Tahirovic S, Dupraz S, Stern S, Garvalov BK, Gurniak C, Shaw AE, Meyn L, Wedlich-Soldner R, Bamburg JR, Small JV, Witke W, and Bradke F (2012) ADF/cofilin-mediated actin retrograde flow directs neurite formation in the developing brain. Neuron 76, 1091–1107 [PubMed: 23259946]

46. Rust MB (2015) ADF/cofilin: a crucial regulator of synapse physiology and behavior. Cell Mol Life Sci 72, 3521–3529 [PubMed: 26037722]
47. Berridge MJ, Lipp P, and Bootman MD (2000) The versatility and universality of calcium signalling. Nat Rev Mol Cell Biol 1, 11–21 [PubMed: 11413485]
48. Greer PL, and Greenberg ME (2008) From synapse to nucleus: calcium-dependent gene transcription in the control of synapse development and function. Neuron 59, 846–860 [PubMed: 18817726]
49. Simons C, Benkert J, Deuter N, Poetschke C, Pongs O, Schneider T, Duda J, and Liss B (2019) NCS-1 Deficiency Affects mRNA Levels of Genes Involved in Regulation of ATP Synthesis and Mitochondrial Stress in Highly Vulnerable Substantia nigra Dopaminergic Neurons. Front Mol Neurosci 12, 252 [PubMed: 31827421]
50. Grosshans HK, Fischer TT, Steinle JA, Brill AL, and Ehrlich BE (2020) Neuronal Calcium Sensor 1 is up-regulated in response to stress to promote cell survival and motility in cancer cells. Mol Oncol 14, 1134–1151 [PubMed: 32239615]
51. Schaad NC, De Castro E, Nef S, Hegi S, Hinrichsen R, Martone ME, Ellisman MH, Sikkink R, Rusnak F, Sygush J, and Nef P (1996) Direct modulation of calmodulin targets by the neuronal calcium sensor NCS-1. Proc Natl Acad Sci U S A 93, 9253–9258 [PubMed: 8799187]
52. Nakamura TY, Jeromin A, Mikoshiba K, and Wakabayashi S (2011) Neuronal calcium sensor-1 promotes immature heart function and hypertrophy by enhancing Ca2+ signals. Circ Res 109, 512–523 [PubMed: 21737792]
53. Kobayashi M, Masaki T, Hori K, Masuo Y, Miyamoto M, Tsubokawa H, Noguchi H, Nomura M, and Takamatsu K (2005) Hippocalcin-deficient mice display a defect in cAMP response element-binding protein activation associated with impaired spatial and associative memory. Neuroscience 133, 471–484 [PubMed: 15878804]
54. Luo L (2000) Rho GTPases in neuronal morphogenesis. Nat Rev Neurosci 1, 173–180 [PubMed: 11257905]
55. Takemura M, Mishima T, Wang Y, Kasahara J, Fukunaga K, Ohashi K, and Mizuno K (2009) Ca2+/calmodulin-dependent protein kinase IV-mediated LIM kinase activation is critical for calcium signal-induced neurite outgrowth. J Biol Chem 284, 28554–28562 [PubMed: 19696021]
56. Saneyoshi T, and Hayashi Y (2012) The Ca2+ and Rho GTPase signaling pathways underlying activity-dependent actin remodeling at dendritic spines. Cytoskeleton (Hoboken) 69, 545–554 [PubMed: 22566410]
57. Weiss JL, Hui H, and Burgoyne RD (2010) Neuronal calcium sensor-1 regulation of calcium channels, secretion, and neuronal outgrowth. Cell Mol Neurobiol 30, 1283–1292 [PubMed: 21104311]
58. Apasu JE, Schuette D, LaRanger R, Steinle JA, Nguyen LD, Grosshans HK, Zhang M, Cai WL, Yan Q, Robert ME, Mak M, and Ehrlich BE (2019) Neuronal calcium sensor 1 (NCS1) promotes motility and metastatic spread of breast cancer cells in vitro and in vivo. FASEB J 33, 4802–4813 [PubMed: 30592625]
59. Nguyen LD, Nolte LG, Tan WJT, Giuvelis D, Santos-Sacchi J, Bilsky E, and Ehrlich BE (2021) Comprehensive somatosensory and neurological phenotyping of NCS1 knockout mice. Sci Rep 11, 2372 [PubMed: 33504822]
60. Penzes P, Cahill ME, Jones KA, VanLeeuwen JE, and Woolfrey KM (2011) Dendritic spine pathology in neuropsychiatric disorders. Nat Neurosci 14, 285–293 [PubMed: 21346746]
61. Reynolds AJ, Bartlett SE, and Morgans C (2001) The distribution of neuronal calcium sensor-1 protein in the developing and adult rat retina. Neuroreport 12, 725–728 [PubMed: 11277572]
62. Treloar HB, Uboha U, Jeromin A, and Greer CA (2005) Expression of the neuronal calcium sensor protein NCS-1 in the developing mouse olfactory pathway. J Comp Neurol 482, 201–216 [PubMed: 15611992]
63. Kawasaki T, Nishio T, Kurosawa H, Roder J, and Jeromin A (2003) Spatiotemporal distribution of neuronal calcium sensor-1 in the developing rat spinal cord. J Comp Neurol 460, 465–475 [PubMed: 12717707]

64. Couillard-Despres S, Winner B, Schaubeck S, Aigner R, Vroemen M, Weidner N, Bogdahn U, Winkler J, Kuhn HG, and Aigner L (2005) Doublecortin expression levels in adult brain reflect neurogenesis. Eur J Neurosci 21, 1–14 [PubMed: 15654838]

65. de Rezende VB, Rosa DV, Comim CM, Magno LA, Rodrigues AL, Vidigal P, Jeromin A, Quevedo J, and Romano-Silva MA (2014) NCS-1 deficiency causes anxiety and depressive-like behavior with impaired non-aversive memory in mice. Physiol Behav 130, 91–98 [PubMed: 24631552]

66. Schuette D, Moore LM, Robert ME, Taddei TH, and Ehrlich BE (2018) Hepatocellular Carcinoma Outcome Is Predicted by Expression of Neuronal Calcium Sensor 1. Cancer Epidemiol Biomarkers Prev 27, 1091–1100 [PubMed: 29789326]

67. Bong AHL, Robitaille M, Milevskiy MJG, Roberts-Thomson SJ, and Monteith GR (2020) NCS-1 expression is higher in basal breast cancers and regulates calcium influx and cytotoxic responses to doxorubicin. Mol Oncol 14, 87–104 [PubMed: 31647602]

68. Moore LM, England A, Ehrlich BE, and Rimm DL (2017) Calcium Sensor, NCS-1, Promotes Tumor Aggressiveness and Predicts Patient Survival. Mol Cancer Res 15, 942–952 [PubMed: 28275088]

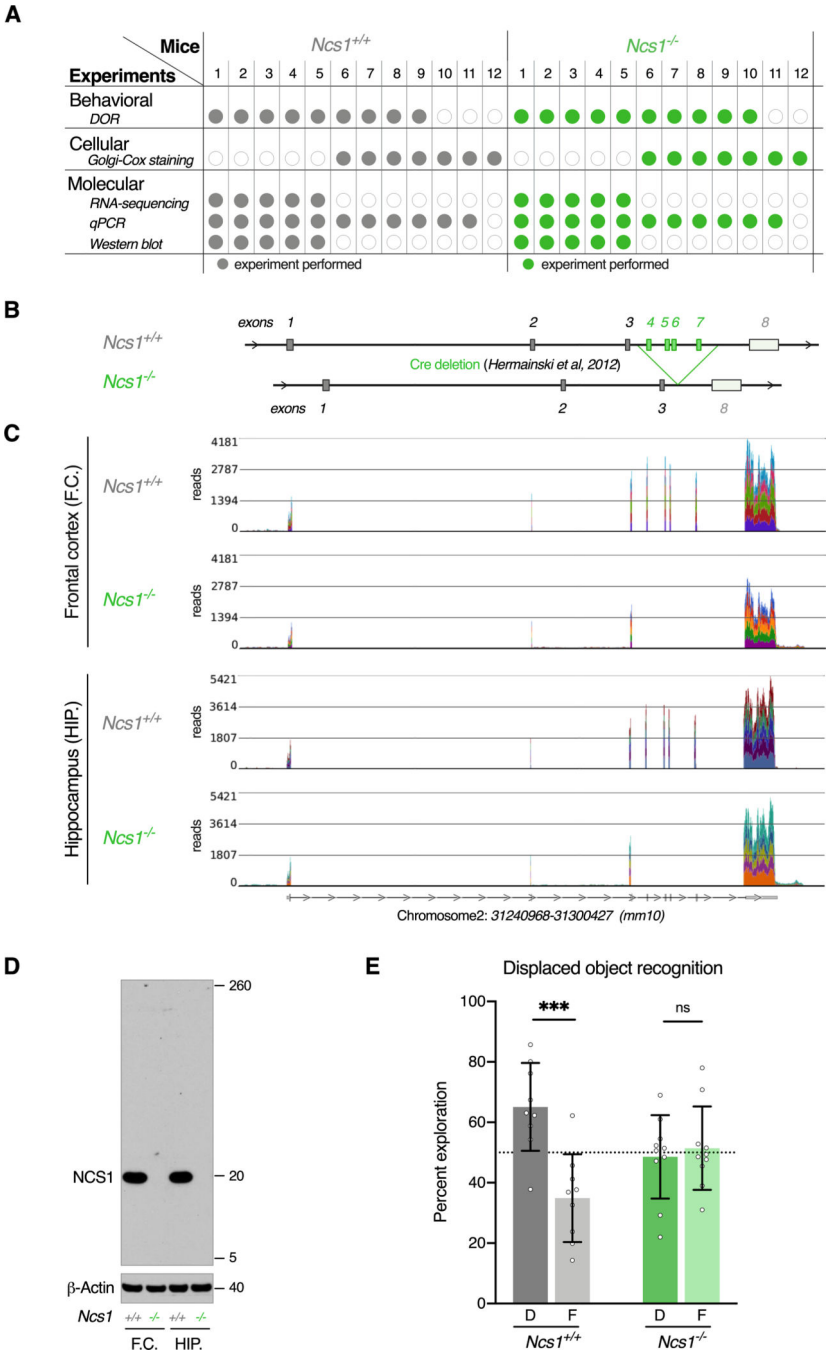

Fig. 1.

Experimental study setup and genetic and behavioral confirmation of the *Ncs1*$^{-/-}$ mouse model. (A) Table showing an overview of experiments performed in this study. *Ncs1*$^{+/+}$ (wildtype, grey, n=12) and *Ncs1*$^{-/-}$ (knockout, green, n=12) mice were compared. Each column represents a single mouse; filled circles indicate that a mouse was included in the corresponding experiment. (B) Schematic diagram of the *Ncs1* gene locus illustrating the generation of the *Ncs1* knockout, adapted from (33, 34). Exons 4, 5, 6, and 7 (green) in the *Ncs1* wildtype locus (top) were deleted through Cre/loxP recombination to create the

knockout strain (bottom). Exon 8 (light grey box) is untranslated. (C) Chromosomal view (aligned to (B)) displaying the *Ncs1* gene locus (mus musculus Chromosome2:31240968–31300427) with stacked RNA-Seq reads obtained from the frontal cortex (F.C.) and hippocampus (HIP.) of $Ncs1^{+/+}$ and $Ncs1^{-/-}$ mice. Y-axis shows the number of read counts, each peak represents one exon, and each color represents one mouse. The absence of exons 4, 5, 6, and 7 in $Ncs1^{-/-}$ mice was confirmed. (D) Western blot confirming the complete loss of NCS1 protein expression in the frontal cortex and hippocampus of $Ncs1^{-/-}$ mice. β-Actin was used as the loading control. (E) Displaced object recognition (DOR) task indicating that $Ncs1^{+/+}$ mice show a significant preference for the displaced object (n=9, unpaired multiple t-test with Holm-Sidak correction, p=0.0009), whereas $Ncs1^{-/-}$ mice do not (n=10, p=0.65); D=displaced, F=familiar.

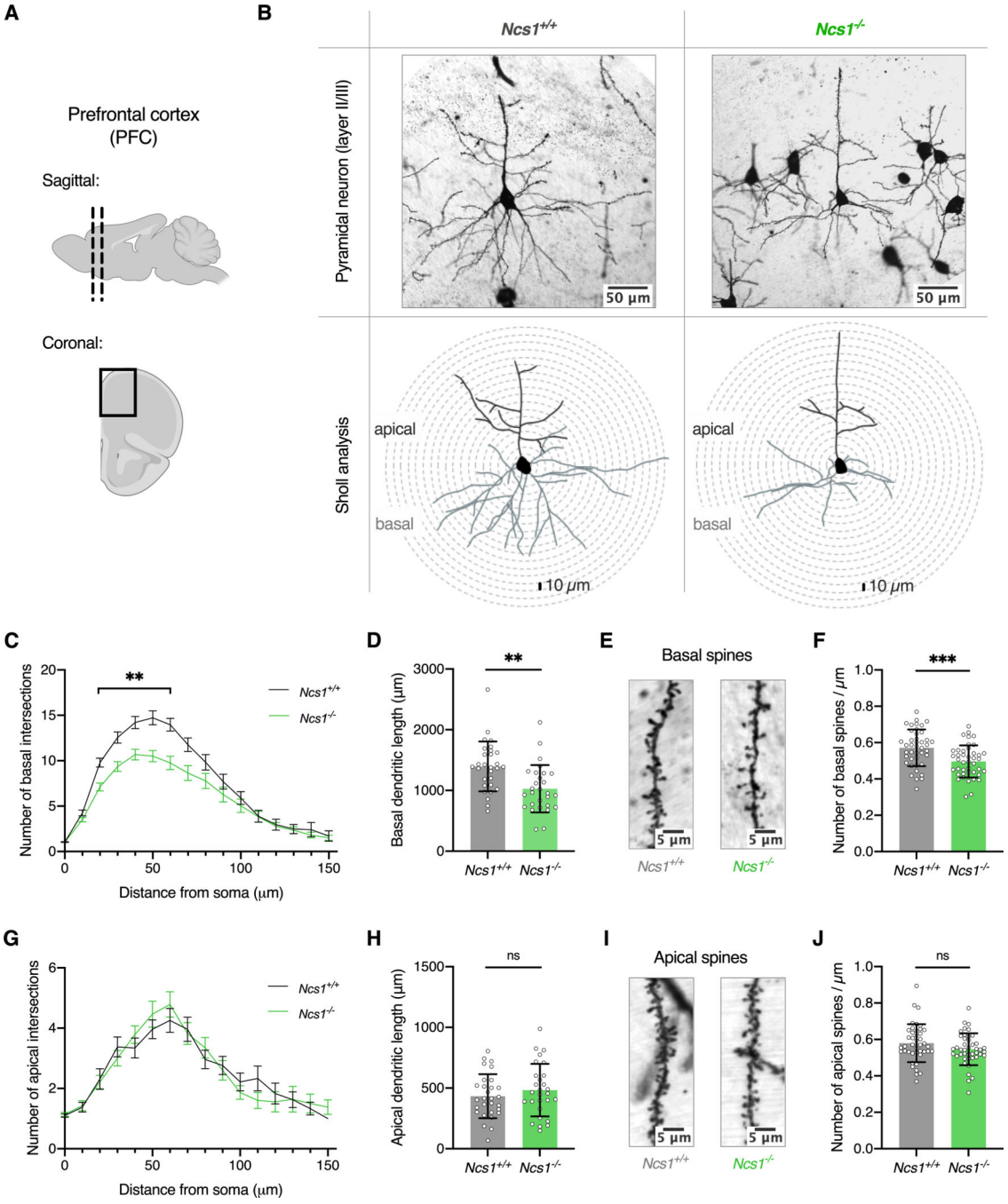

Fig. 2.

Golgi-Cox staining and quantification of layer II/III pyramidal neurons in the prefrontal cortex (PFC) of *Ncs1*$^{-/-}$ and *Ncs1*$^{+/+}$ mice. (A) Schematic diagram depicting the slicing position in sagittal view (upper panel) and the region where the dorsal hippocampus was imaged in a coronal section (lower panel). (B) Table displays representative images of layer II/III neurons from the PFC of *Ncs1*$^{+/+}$ and *Ncs1*$^{-/-}$ mice (upper panels) and the respective skeletonized traces of these neurons as used for Sholl analysis (lower panels). Apical dendrites are shown in black, and basal dendrites are shown in grey. Sholl analysis

was performed by counting the number of dendritic intersections at 10 μm intervals from the soma in concentric circles. (C-D) Sholl analysis and quantification of basal dendrites of layer II/III pyramidal neurons in the PFC; n=7 mice per group, n=4 neurons per mouse. (C) Mean ± SEM is shown; mixed effects two-way ANOVA, Genotype: $F(1, 55)= 8.53$, $p=0.0051$, Genotype x Distance: $F(15, 678)=4.47$, $p<0.0001$; Sidak's multiple comparisons, $p<0.01$ at each interval between 20–60 μm. (D) Two-tailed, unpaired t-test, $p=0.001$. (E-F) Representative images and quantification of basal spine density of layer II/III pyramidal neurons in the PFC; n=7 mice per group, n=6 segments per mouse. (F) Two-tailed, unpaired t-test, $p=0.0005$. (G-H) Sholl analysis and quantification of apical dendrites of layer II/III pyramidal neurons in the PFC; n=7 mice per group, n=4 neurons per mouse. (G) Mean ± SEM is shown; mixed effects two-way ANOVA, Genotype: $F(1, 55)=0.003$, $p=0.96$. (H) Two-tailed, unpaired t-test, $p=0.35$. (I-J) Representative images and quantification of apical spine density of layer II/III pyramidal neurons in the PFC; n=7 mice per group, n=6 segments per mouse. (J) Two-tailed, unpaired t-test, $p=0.11$.

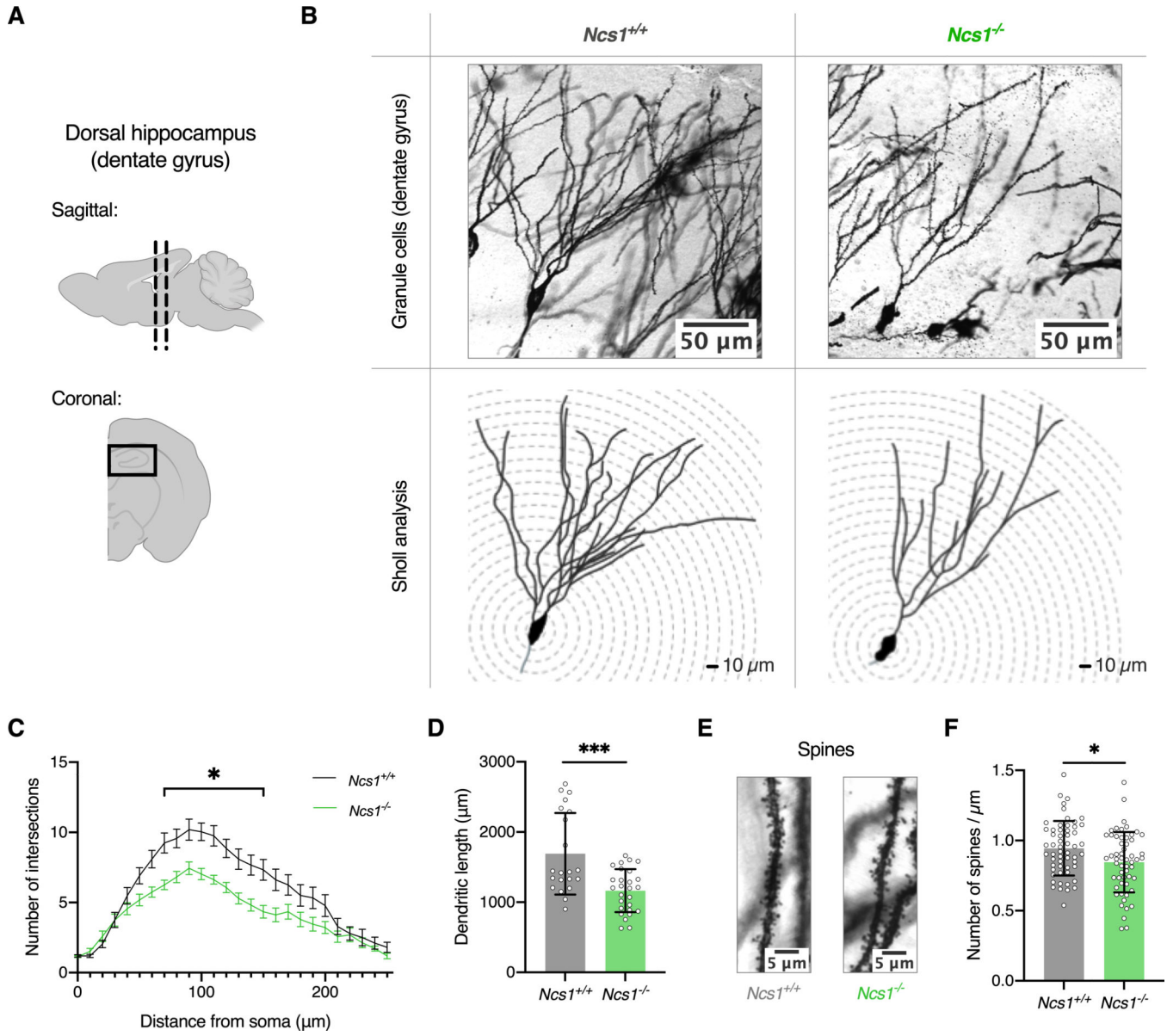

Fig. 3.

Golgi-Cox staining and quantification of granule cells in the dentate gyrus in the dorsal hippocampus of *Ncs1*$^{-/-}$ and *Ncs1*$^{+/+}$ mice. (A) Schematic diagram depicting the slicing position in sagittal view (upper panel) and the region where the dorsal hippocampus was imaged in a coronal section (lower panel). (B) Table displays representative images of granule cells in the dentate gyrus from *Ncs1*$^{+/+}$ and *Ncs1*$^{-/-}$ mice (upper panels) and the respective skeletonized traces of these neurons as used for Sholl analysis (lower panels). Sholl analysis was performed by counting the number of dendritic intersections at 10 µm intervals from the soma in concentric circles. (C-D) Sholl analysis and quantification of dendrites of granule cells; n=7 mice per group, n=3–4 neurons per mouse. (C) Mean ± SEM is shown; mixed effects two-way ANOVA, Genotype: $F(1, 46)=11.85$, $p=0.001$, Genotype x Distance: $F(28, 982)=4.113$, $p<0.0001$; Sidak's multiple comparisons, $p<0.05$ at each

interval between 70–150 μm, except p≤0.1 at 90 and 130 μm. (D) Two-tailed, unpaired t-test, p=0.0002. (E-F) Representative images and quantification of spine density in granule cells; n=7 mice per group, n=8 segments per mouse. (F) Two-tailed, unpaired t-test, p=0.01.

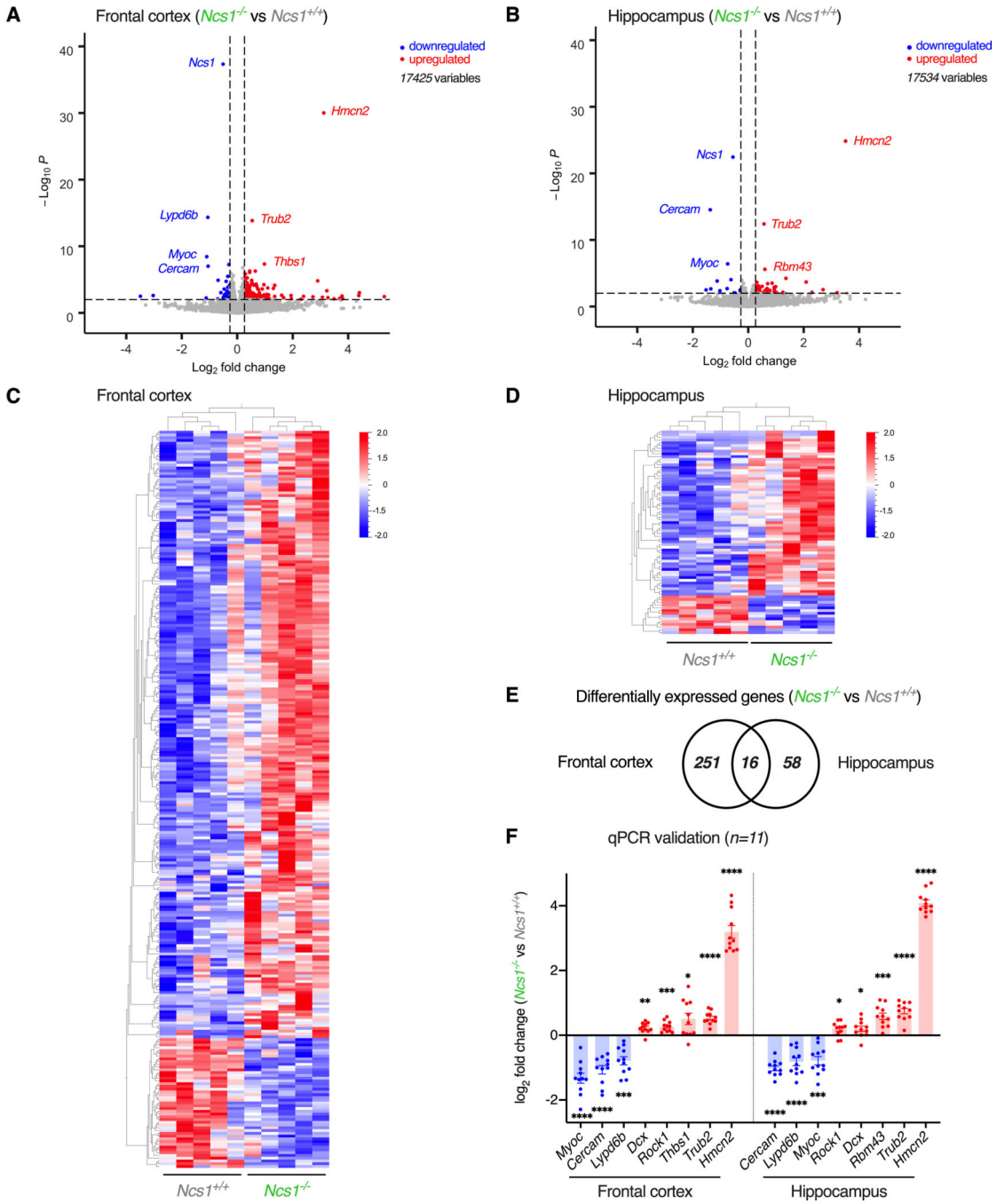

Fig. 4.

Whole-transcriptome RNA-Seq analysis of *Ncs1*$^{-/-}$ and *Ncs1*$^{+/+}$ brain tissues. (A-B) Volcano plots showing differentially expressed genes (DEGs) in *Ncs1*$^{-/-}$ (n=5) compared with *Ncs1*$^{+/+}$ (n=5) mice. The threshold for the fold change (FC) was set at FC ≥ |1.2| ($\log_2$ = |0.26|), and at p-value ≤ 0.01, as represented by the dotted vertical and horizontal lines, respectively. In the frontal cortex, 47 genes were downregulated (blue) and 220 genes were upregulated (red) (A). In the hippocampus, 14 genes were downregulated (blue) and 60 genes were upregulated (red) (B). (C-D) Heat maps showing unsupervised hierarchical

clustering based on log_2-transformed normalized gene expression values for DEGs (267 for frontal cortex, 74 for hippocampus) in *Ncs1*$^{-/-}$ compared with *Ncs1*$^{+/+}$ mice. Each column represents one mouse and each row represents one gene. (E) Venn diagram depicting the overlap of DEGs in the frontal cortex and hippocampus of *Ncs1*$^{-/-}$ compared with *Ncs1*$^{+/+}$ mice. (F) Bar graph showing the log_2FC for the indicated genes in *Ncs1*$^{-/-}$ compared with *Ncs1*$^{+/+}$ mice as measured by real-time quantitative PCR (qPCR). Results from RNA-Seq experiments were validated with technical (n=5) and biological (n=6) replicates; n=11 per genotype; one sample t-test compared to 0, frontal cortex (*Myoc*: p<0.0001, *Cercam*: p<0.0001, *Lypd6b*: p=0.0001, *Dcx*: p=0.0011, *Rock1*: p=0.0003, *Thbs1*: p=0.015, *Trub2*: p<0.0001, *Hmcn2*: p<0.0001), hippocampus (*Cercam*: p<0.0001, *Lypd6b*: p<0.0001, *Myoc*: p<0.0001, *Rock1*: p=0.015, *Dcx*: p=0.032, *Rbm43*: p=0.0002, *Trub2*: p<0.0001, *Hmcn2*: p<0.0001).

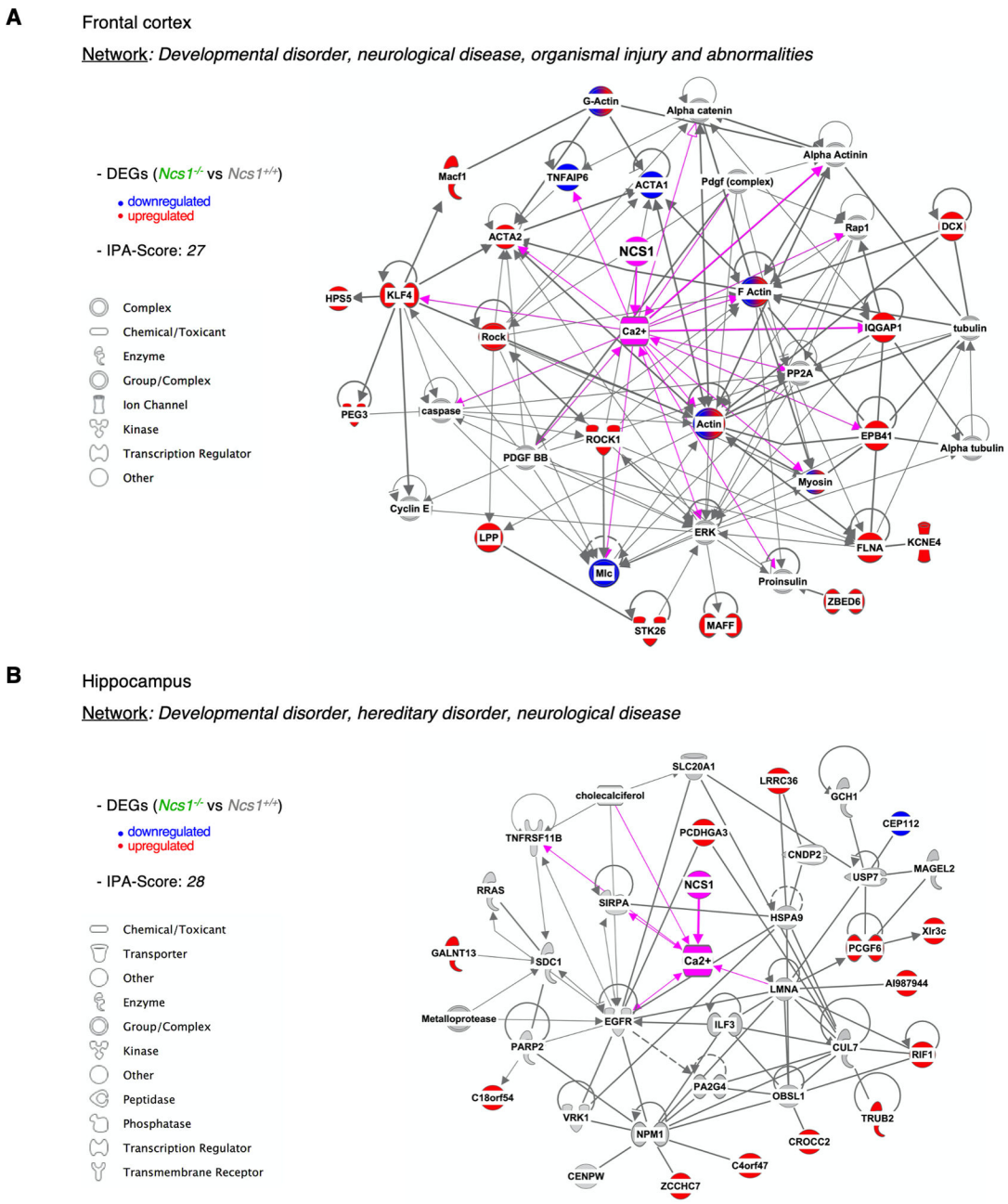

Fig. 5.

Functional network analysis of DEGs identified in *Ncs1*$^{-/-}$ compared with *Ncs1*$^{+/+}$ mice. Functional networks with 35 nodes were generated de novo based on the DEGs in *Ncs1*$^{-/-}$ mice using the automated IPA network generation algorithm. DEGs that are part of the network are shown in blue (downregulated) or red (upregulated) according to their fold change in the RNA-Seq experiments. Grey nodes were automatically added from Ingenuity Knowledge Base to specifically connect two or more smaller networks by merging them into a larger one. Edges (lines and arrows between nodes) represent direct (bold lines) and

indirect (thin lines) interactions between molecules, as supported by experimental data in the Ingenuity Knowledge Base. *NCS1* (pink) was added to the networks post-hoc and, through intermediate molecules, connected to the network. (A) For the cortex, the functional network "Developmental disorder, neurological disease, organismal injury and abnormalities" with an IPA Score of 27 is shown. 23 DEGs are part of this network. The molecule connecting NCS1 to the largest number of network nodes was Ca2+. Other intermediate molecules include HTT, MAPK1, cAMP, and DRD2/3. (B) For the hippocampus, the functional network "Developmental disorder, hereditary disorder, neurological disease" with an IPA Score of 28 is shown. 13 DEGs are part of this network. The molecule connecting NCS1 to the largest number of network nodes was Ca2+. Other intermediate molecules include ITPR1, HTT, MAPK1, TRAF2, cAMP, SPP1, and DRD2.

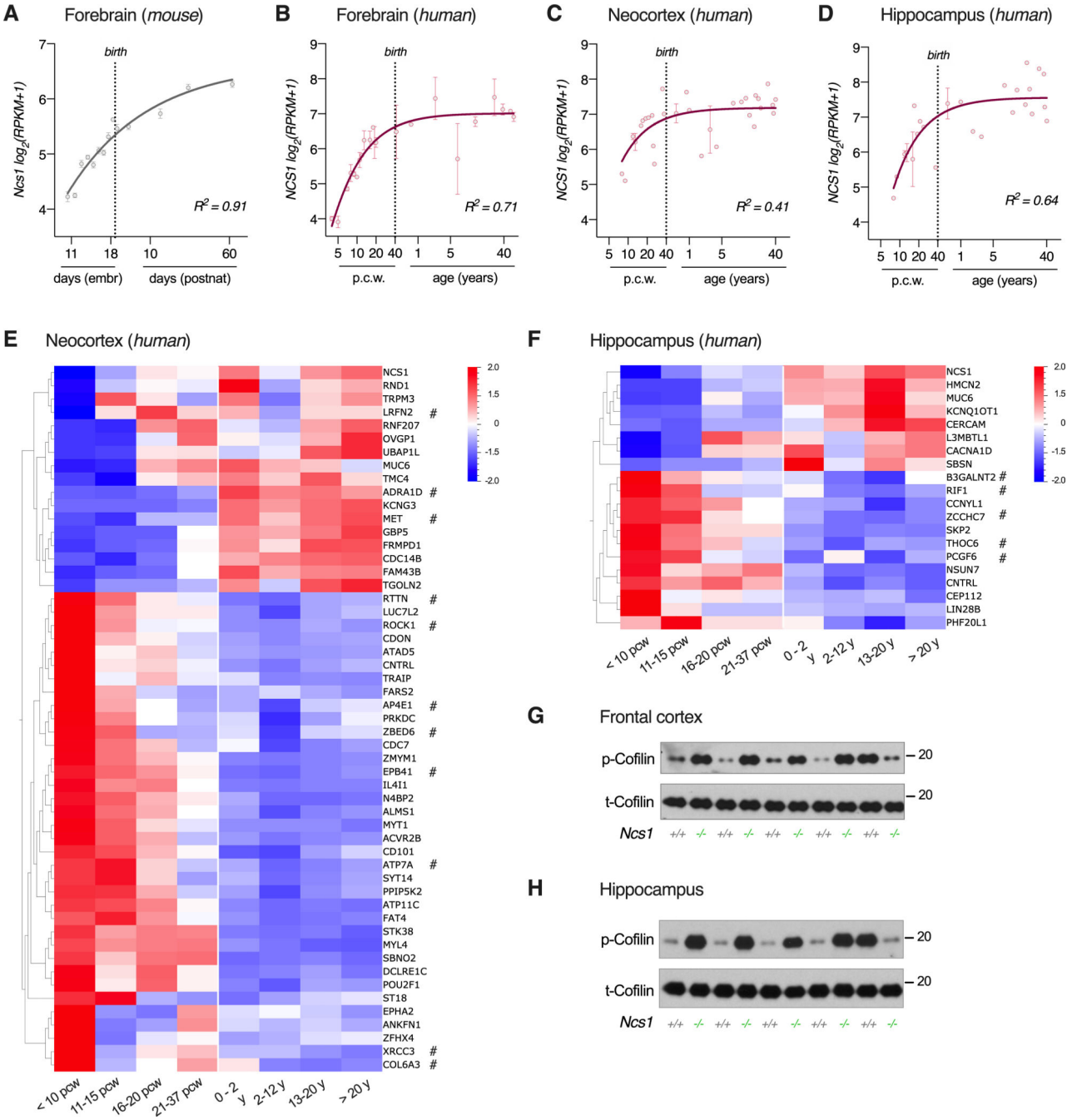

Fig. 6.

NCS1 expression levels during brain development. Gene expression data for *Ncs1* and DEGs identified in *Ncs1*$^{-/-}$ mice were retrieved from publicly available databases (Kaessmann Lab data set (A-B) and BrainSpan data set (C-F)). (A-D) Scatter blots showing the trajectories of $\log_2$-transformed *Ncs1* gene expression in mouse and *NCS1* gene expression in human brain tissues over time on a $\log_{10}$-transformed time scale. For each time point, the mean ± SEM is shown. Non-linear regression was applied. (A) Mouse forebrain, embryonic day 10.5 to postnatal day 63, n=3–4 per time point, three-point fit, R^2=0.91. (B) Human forebrain,

4 weeks post-conception (p.c.w.) to 60 years of age, n=1–4 per time point, three-point fit, R^2=0.71. (C) Human neocortex, 8 weeks p.c.w. to 40 years of age, n=1–3 per time point, three-point fit, R^2=0.41. (D) Human hippocampus, 8 weeks p.c.w. to 40 years of age, n=1–3 per time point, three-point fit, R^2=0.64. (E-F) Heat maps showing the trajectories of log_2-transformed normalized gene expression for *NCS1* and DEGs that show a strong correlation (r > |0.7|) with *NCS1* in the BrainSpan data set over time. 53 genes in the frontal cortex (E) and 20 genes in the hippocampus (F) are highly correlated with *Ncs1*. Samples were grouped into 4 prenatal and 4 postnatal groups as indicated below the heat map. # indicates that the gene has been associated with neurodevelopmental disorders in the Ingenuity Knowledge Base or was part of the functional networks shown in Fig. 5, y = years. (G-H) Western blots showing the abundance of p-Cofilin in the frontal cortex (G) and the hippocampus (H) of $Ncs1^{+/+}$ and $Ncs1^{-/-}$ mice; t-Cofilin was used as the loading control; n=5 per group.

Table 1.

Top Diseases and Bio Functions enriched in the 267 DEGs identified in the Frontal Cortex of *Ncs1*$^{-/-}$ mice.

A - Molecular and Cellular Functions		
Name	**p-value range**	**# Molecules (/ 267)**
Cellular Assembly and Organization	$1.17x10^{-3}$ – $1.94x10^{-7}$	52
Cellular Movement	$1.34x10^{-3}$ – $2.39x10^{-7}$	62
Cell-To-Cell Signaling and Interaction	$1.34x10^{-3}$ – $7.81x10^{-7}$	37
Cell Morphology	$1.34x10^{-3}$ – $8.68x10^{-7}$	25
Cellular Development	$1.03x10^{-3}$ – $4.14x10^{-6}$	51
B - Diseases and Disorders		
Name	**p-value range**	**# Molecules (/ 267)**
Cancer	$1.34x10^{-3}$ – $3.24x10^{-14}$	205
Organismal Injury and Abnormalities	$1.34x10^{-3}$ – $3.24x10^{-14}$	212
Reproductive System Disease	$9.50x10^{-4}$ – $1.20x10^{-13}$	170
Gastrointestinal Disease	$1.34x10^{-3}$ – $7.56x10^{-13}$	205
Neurological Disease	$1.25x10^{-3}$ – $2.22x10^{-11}$	140
C - Physiological System Development and Function		
Name	**p-value range**	**# Molecules (/ 267)**
Cardiovascular System Development and Function	$1.22x10^{-3}$ – $4.84x10^{-9}$	58
Organismal Development	$1.22x10^{-3}$ – $5.27x10^{-8}$	62
Tissue Development	$1.24x10^{-3}$ – $1.94x10^{-7}$	67
Connective Tissue Development and Function	$1.34x10^{-3}$ – $2.39x10^{-7}$	39
Embryonic Development	$1.15x10^{-3}$ – $5.74x10^{-7}$	56

Table 2.

Top Diseases and Bio Functions enriched in the 74 DEGs identified in the Hippocampus of *Ncs1*$^{-/-}$ mice.

A - Molecular and Cellular Functions		
Name	**p-value range**	**# Molecules (/ 74)**
Cellular Function and Maintenance	$2.44x10^{-2}$ – $2.20x10^{-4}$	13
Molecular Transport	$2.00x10^{-2}$ – $2.20x10^{-4}$	10
Cell Morphology	$2.44x10^{-3}$ – $4.05x10^{-4}$	12
Carbohydrate Metabolism	$1.78x10^{-3}$ – $5.81x10^{-4}$	5
Lipid Metabolism	$1.78x10^{-3}$ – $5.81x10^{-4}$	4
B - Diseases and Disorders		
Name	**p-value range**	**# Molecules (/ 74)**
Cancer	$2.41x10^{-2}$ – $1.32x10^{-4}$	47
Organismal Injury and Abnormalities	$2.44x10^{-2}$ – $1.32x10^{-4}$	47
Reproductive System Disease	$2.21x10^{-2}$ – $1.32x10^{-4}$	40
Cardiovascular Disease	$2.44x10^{-2}$ – $1.76x10^{-4}$	5
Neurological Disease	$2.00x10^{-3}$ – $1.76x10^{-4}$	14
C - Physiological System Development and Function		
Name	**p-value range**	**# Molecules (/ 74)**
Organ morphology	$2–22x10^{-2}$ – $9.79x10^{-5}$	10
Organismal Development	$2.44x10^{-2}$ – $9.79x10^{-5}$	19
Digestive System Development and Function	$2.44x10^{-2}$ – $1.84x10^{-4}$	10
Organismal Functions	$9.14x10^{-4}$ – $9.14x10^{-4}$	2
Cardiovascular System Development and Function	$2.00x10^{-2}$ – $1.11x10^{-3}$	12